

1 A general substitution matrix for structural phylogenetics.  
2

3 Sriram G Garg<sup>1</sup> and Georg KA Hochberg<sup>1,2,3</sup>  
4

5 1 Max Planck Institute for Terrestrial Microbiology, Karl-von-Frisch-Straße 10, 35043  
6 Marburg, Germany.

7 2 Center for Synthetic Microbiology (SYNMIKRO), Philipps-University Marburg; Karl-von-  
8 Frisch-Str. 14, 35043 Marburg, Germany

9 3 Department of Chemistry, Philipps-University Marburg; Hans-Meerwein-Str. 4, 35043  
10 Marburg, Germany

11 Correspondence to: georg.hochberg@mpi-marburg.mpg.de  
12

## 14 Abstract

15 Sequence-based maximum likelihood (ML) phylogenetics is a widely used method for  
16 inferring evolutionary relationships, which has illuminated the evolutionary histories of  
17 proteins and the organisms that harbour them. But modern implementations with  
18 sophisticated models of sequence evolution struggle to resolve deep evolutionary  
19 relationships, which can be obscured by excessive sequence divergence and substitution  
20 saturation. Structural phylogenetics has emerged as a promising alternative, because  
21 protein structure evolves much more slowly than protein sequences. Recent developments  
22 in protein structure prediction using AI have made it possible to predict protein structures for  
23 entire protein families, and then to translate these structures into a sequence  
24 representation - the 3Di structural alphabet - that can in theory be directly fed into existing  
25 sequence based phylogenetic software. To unlock the full potential of this idea, however,  
26 requires the inference of a general substitution matrix for structural phylogenetics, which  
27 has so far been missing. Here we infer this matrix from large datasets of protein structures  
28 and show that it results in a better fit to empirical datasets than previous approaches. We  
29 then use this matrix to re-visit the question of the root of the tree of life. Using structural  
30 phylogenies of universal paralogs, we provide the first unambiguous evidence for a root  
31 between archaea and bacteria. Finally, we discuss some practical and conceptual  
32 limitations of structural phylogenetics. Our 3Di substitution matrix provides a starting point  
33 for revisiting many deep phylogenetic problems that have so far been extremely difficult to  
34 solve.

35  
36  
37 **Keywords:** Phylogenetics, Maximum likelihood, Structural phylogenetics, evolution,  
38 substitution models

## 39 40 Introduction

41 The field of phylogenetics has evolved from relying on morphological comparisons to  
42 sophisticated sequence-based analyses (Whelan et al., 2001). The advent of  
43 computational methods marked a turning point, introducing a range of algorithms from  
44 Neighbour-Joining (NJ) (Saitou and Nei, 1987) and Maximum Parsimony (MP) (Farris, 1970;  
45 Fitch 1971) to Maximum Likelihood (ML) (Felsenstein, 1981) and Bayesian inferences  
46 (Rannala and Yang, 1996; Mau and Newton, 1997) on nucleotide and amino acid

48 sequences. Each methodological leap has brought with it a deeper understanding of  
49 evolutionary history through better trees. Among the various phylogenetic methods,  
50 Maximum Likelihood (ML) approaches have emerged as particularly powerful tools for  
51 modelling evolutionary processes (Posada and Crandall, 2021). The flexibility and  
52 robustness of ML techniques have made them indispensable for contemporary  
53 phylogenetic studies, especially those tackling large datasets or seeking to resolve deep  
54 evolutionary relationships. But especially deep, sequenced-based phylogenetics remains  
55 difficult. Substitution saturation is a particular challenge, in which each site in the  
56 alignment has accumulated multiple substitutions over a branch of interest (Brown, 1982,  
57 Phillippe and Forterre 1999). Depending on the accuracy of the substitution model of  
58 sequence evolution, saturation can lead to spurious phylogenetic signals and artefacts in  
59 phylogenetic trees (Felsenstein, 2003). The problem of saturation cannot always be solved  
60 by adding more sequences (Philippe et al., 2011) or better models of sequence evolution.  
61

62 Saturation is a relevant problem for the identification of the root of the tree of life. It is  
63 traditionally placed on the branch between bacteria and archaea (Gouy et al., 2015), which  
64 has important implications for the nature of the Last Universal Common Ancestor (LUCA).  
65 This inference is based on paralog rooting with universally duplicated genes, where the  
66 paralogs reciprocally root each other (Iwabe et al., 1989). Although this root is tacitly  
67 accepted by the majority of biologists, the paralog trees it is based on are riddled with  
68 potential problems. In all previous attempts, the branch between universal paralogs  
69 remains so long as to be probably saturated (Brown and Doolittle, 1995; Philippe and  
70 Forterre, 1999; Gouy et al., 2015; Mahendarajah et al., 2023). This means that the root  
71 position within each paralog might be mostly determined by the preferences of the  
72 substitution model, rather than real phylogenetic signal, which has been erased almost  
73 entirely. Some phylogenetics therefore still consider the root of the tree of life an unsolved  
74 problem (Gouy et al., 2015).  
75

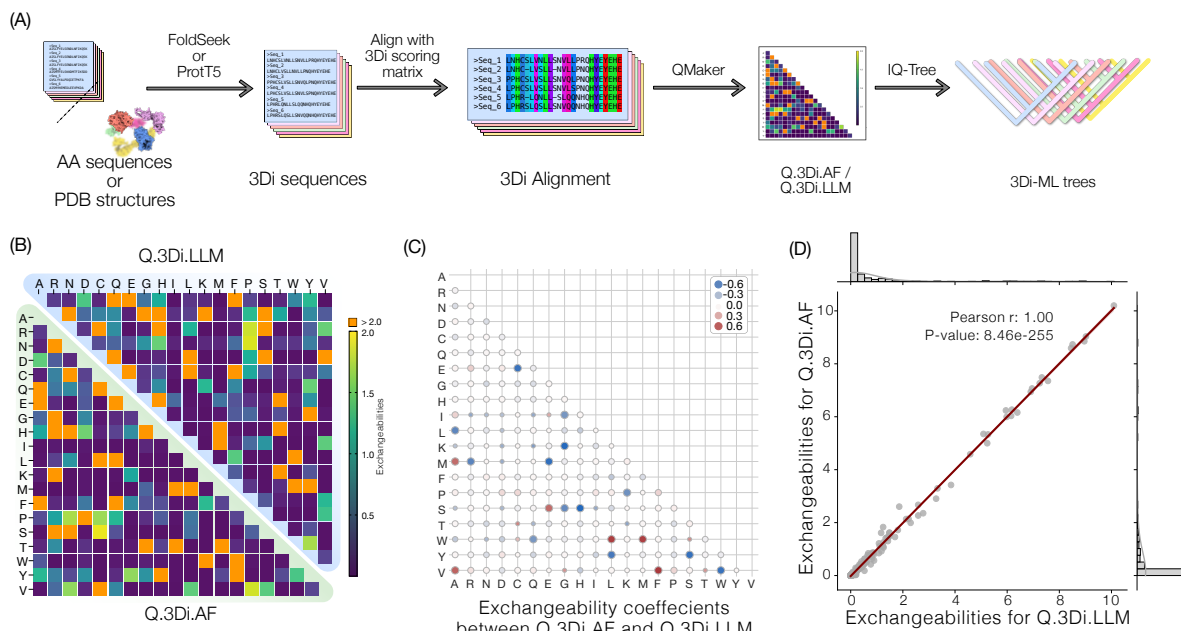
76 Structural phylogenetics offers a potentially powerful alternative to traditional sequence-  
77 based approaches. Structures evolve much more slowly than sequences, and if a model  
78 for structural evolution could be inferred, this could help resolve phylogenies that are  
79 beyond the reach of sequenced-based methods. Early attempts at this idea were limited by  
80 the lack of high-quality protein structures or reliable methods of scoring multiple sequence  
81 alignments of protein structures (Johnson, Šali, et al., 1990; Johnson et al., 1990; Balaji et  
82 al., 2001; Balaji and Srinivasan, 2001). This changed with the advent of artificial intelligence  
83 models that can predict protein structures with good accuracy (Jumper et al., 2021; Varadi  
84 et al., 2023). The availability of a large database of structures has prompted researchers to  
85 mould this novel source of information for identification of structural homologs in a process  
86 similar to BLAST. Chief among these tools is FoldSeek which translates the 3D information  
87 in predicted and experimentally determined structures into 20 unique characters the  
88 authors call the 3Di alphabet (Kempen et al., 2023). The advantage of using an alphabet of  
89 20 characters is that it enables the direct use of these 3Di characters in conventional  
90 implementations of amino acid-based likelihood methods.  
91

92 The conversion of a large dataset of 3D structures into the 3Di alphabet allows the  
93 computation of a scoring matrix like the BLOSUM scoring matrix commonly employed by  
94 Multiple Sequence Alignment programs (Kempen et al., 2023). This scoring matrix enables

95 the quick identification of structural homologs of proteins which has been very successful  
96 in the identification of divergent orthologs. Such a scoring system also allows to compute a  
97 similarity score (*fident* in case of FoldTree) which can then be used to compute Neighbour  
98 Joining (NJ) trees as demonstrated by FoldTree (Moi et al., 2023). Furthermore, one could  
99 also calculate a substitution matrix from this BLOSUM style scoring matrix which can be  
100 directly implemented in ML approaches such as in the case of 3DiPhy (Puente-Lelievre et  
101 al., 2024). Neither of these approaches correspond to standard maximum likelihood  
102 phylogenetics for amino acids: FoldTree's neighbour joining method is fast and simple but  
103 inherits all limitations of classical neighbour joining in that it relies on the true distance  
104 between sequences being close to their observed distance (an assumption that is often  
105 violated in realistic datasets) and it does not account for among site rate variation  
106 (Mihaescu et al., 2009). 3DiPhy does use a full likelihood model, which can account for  
107 these phenomena however, its substitution matrix is derived from a BLOSUM-like  
108 alignment scoring matrix. Such matrices are constructed by counting co-occurrences of  
109 particular characters in sequence pairs, rather than inferring their contents using maximum  
110 likelihood (Le and Gascuel, 2008). In standard sequence phylogenetics the BLOSUM matrix  
111 has long been superseded by empirical models which are inferred in a full phylogenetic  
112 likelihood framework, and generally result in a much better fit to empirical data (Le and  
113 Gascuel, 2008).

114  
115 These features of existing structural phylogenetics frameworks motivated us to infer a new  
116 substitution model using a phylogenetic maximum likelihood framework. This substitution  
117 model can in theory be directly inferred from each alignment in the form of a General Time  
118 Reversible (GTR) model but inferring a substitution matrix for a 20-letter alphabet from a  
119 single multiple sequence alignment is difficult and prone to overfitting. For conventional  
120 protein models, this problem is solved by combining large numbers of protein alignments  
121 and inferring from them one substitution model that best describes all the data. Once  
122 computed, this general model, also denoted as  $Q$ , can then be used for individual protein  
123 families, which avoids overfitting using GTR. Here we make use of AlphaFold and a recently  
124 developed protein large language model to infer a general substitution matrix for structural  
125 phylogenetics. We show that this  $Q$ -matrix outperforms all previous methods to use 3Di  
126 characters to infer ML phylogenies. Finally, we use our  $Q$ -matrix to re-infer the phylogenies  
127 of universal paralogs and photosystems to settle long-standing questions in deep evolution  
128 that previously suffered from saturation.

129  
130  
131



132  
133 *Figure 1: (A) Overview of the pipeline employed in the manuscript. Briefly, Amino acid (AA) or PDB structures*  
134 *were translated into 3Di characters using FoldSeek or the bilingual ProtT5 model. These 3Di characters are*  
135 *aligned with MAFFT using the 3Di scoring matrix before being used to estimate the general substitution Q-*  
136 *matrix using QMaker which were subsequently used to estimate 3Di-ML trees using IQ-tree. (B) Lower*  
137 *triangular portion is a representation of the Q-matrix estimated from 1660 AF clusters while the upper*  
138 *triangular section denotes the Q matrix estimated from 6653 PFAM clusters translated to 3Di alphabet using*  
139 *the ProtT5 bilingual language model. In both cases values higher than 2 are coloured orange. (C) Ratio of*  
140 *exchangeabilities between the Q.3Di.AF and the Q.3Di.LLM matrix. Each square represents the value  $(m_1^{ij} -$*   
141  *$m_2^{ij}) / (m_1^{ij} + m_2^{ij})$  where  $m_1$  and  $m_2$  represent Q.3Di.AF and Q.3Di.LLM respectively. (D) Pearson's correlation*  
142 *between the exchangeabilities of the two matrices indicating very little differences between the two matrices*

## 143 Results and Discussion

### 144 Estimation of the 3Di Q-matrix

145 We set out to compute a general Q-matrix for structural phylogenetics. Given a large  
146 enough dataset, this is straightforward to achieve using the QMaker routine of IQ tree (Minh  
147 et al., 2021). We used two strategies to gather a large dataset of protein families and their  
148 predicted structures. Our first goal was to use the set of 6653 protein families that was used  
149 to infer a Q matrix in the initial study by Minh et al. To avoid having to predict AlphaFold  
150 models for every sequence in this large database, we opted to use a recently developed  
151 bilingual large language model, ProtT5. This model was trained to directly translate between  
152 an amino acid sequence and its corresponding 3Di sequence, without having to infer an  
153 AlphaFold model (Heinzinger et al., 2023). We used this method to translate all sequences  
154 in the PFAM dataset from AA-sequences to 3Di. The ProtT5 model is not perfect, as it  
155 introduces some randomness into the 3Di translation, meaning that translating to a 3Di  
156 sequence from the same input amino acid sequence results in a slightly different prediction  
157 (Supplementary Figure 1A-C). In addition, when comparing 3Di sequences extracted from  
158 AlphFold2 structures to the same 3Di sequence predicted with the LLM model, we found  
159 large numbers of sequences in which the AlphaFold and LLM predictions had low pairwise  
160 identities (Supplementary Figure 1D-F, Supplementary Figure 2). In order to safeguard  
161 against potential errors in estimating the substitution model using incorrectly translated 3Di  
162 sequences, we used a combination of both ProtT5 and AlphaFold2 predictions to estimate the  
163 Q-matrix. This approach resulted in a Q-matrix that was very similar to the one estimated  
164 using only AlphaFold2 predictions (Supplementary Figure 1G-H). The resulting Q-matrix

165 sequences we also estimated a separate Q matrix using 3Di sequences extracted from  
166 AlphaFold predictions. We employed FoldSeek to cluster the SwissProt AlphaFold  
167 Database. These 1660 AF clusters (hereafter AF-db) were used along with 3Di translation  
168 of the 6653 protein families (hereafter Pfam-db), for the QMaker pipeline. Crucially, both  
169 sets of 3Di sequences were then aligned using the alignment program *mafft* using the 3Di  
170 scoring matrix from (Kempen et al., 2023) instead of the standard BLOSUM62 matrix used  
171 for amino acid alignments.

172  
173 We then estimated a tree for each of 3Di Multiple Sequence Alignments (MSAs) in our two  
174 datasets using the GTR20 model despite the concern of model overfitting given the unique  
175 nature of the 3Di alphabet and the lack of other models that could serve as the initial  
176 starting model. These initial trees were then used to estimate a single Q-matrix that best  
177 explains the respective sets of MSAs as described in the QMaker pipeline (Minh et al., 2021).  
178 This resulted in two Q-matrixes hereafter denoted as Q.3Di.AF and Q.3Di.LLM. The two Q-  
179 matrices estimated were very similar with minor differences in exchangeabilities (Figure 1C)  
180 with a Pearsons correlation of 1 (Figure 1D). We then checked if these matrices are  
181 preferred by IQ-Tree's *modelfinder* over the GTR20 or the previously published 3DiPhy  
182 model using a test set of 6653 3Di MSAs from PFAM that were not used for estimating the  
183 Q-matrix. Indeed, the 3DiPhy model is only preferred in 278 MSAs over 6267 MSAs that  
184 prefer either the Q.3Di.AF or the Q.3Di.LLM model, which are practically the same (Figure  
185 1B-D). This increased our confidence that we had successfully captured the mechanism of  
186 change describing the mutability in the structural alphabet across a wide range of proteins.  
187 In the analyses of specific protein families that follow, IQ-Tree's *modelfinder* predominantly  
188 chose Q.3Di.AF over Q.3Di.LLM or GTR20 according to the Corrected Akaike Criterion  
189 (AICc). Generally, we encourage future users of these matrices to always test if using  
190 Q.3Di.AF changes any conclusions in cases where Q.3Di.LLM is the better fit model. This is  
191 because the AF matrix is much less affected by the misprediction issues than the LLM  
192 (which we discuss further below).  
193

Model	AICc	AIC	BIC
Q.3Di.AF	2342	2065	2309
Q.3Di.LLM	3925	2958	3697
3DiPhy	278	322	267
GTR20	108	1308	380
<i>Total</i>	6653	6653	6653

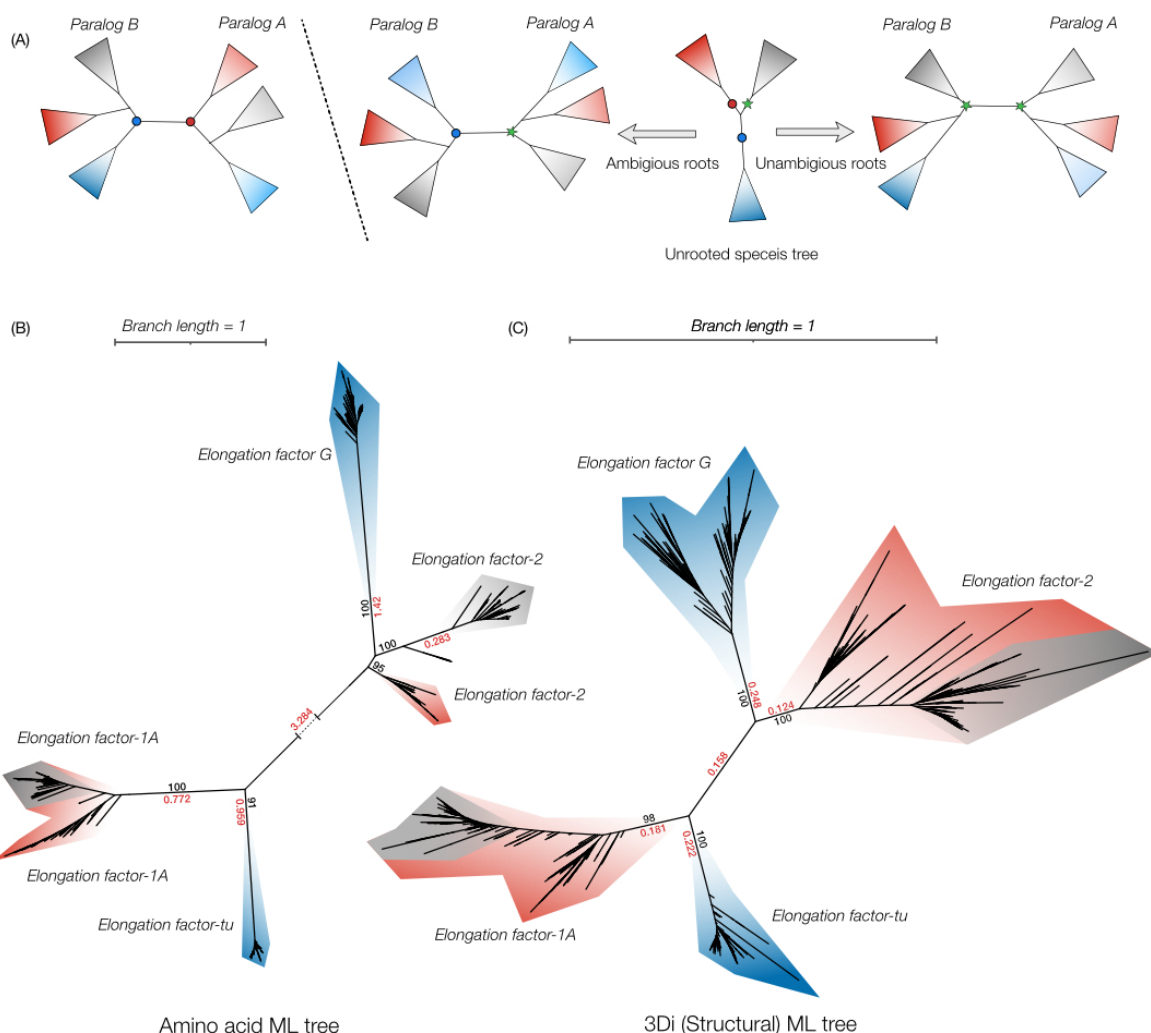
194  
195 Table 1: Number of trees that preferred each model/Q-matrix as identified using *modelfinder* from IQ-Tree  
196 according to corrected Akaike Information Criterion (AICc), Akaike Information Criterion (AIC) and Bayesian  
197 Information Criterion (BIC)

198  
199 *Rooting the ToL using structural phylogenetics*

200  
201 Rooting the tree of life is a particularly challenging problem owing to the lack of outgroups  
202 that can reliably root phylogenetic trees. Paralog rooting is a powerful method which uses  
203 phylogenetic trees with duplicated genes that reciprocally root each other. In most cases  
204 the paralogs root each other along the same branch recovering an unambiguous root for  
205 the species tree containing the paralogs. However, in cases of highly divergent paralogs,

206 the two paralogs sometimes do not agree on the same root (Figure 2A). We tested if our new  
207 matrix can help improve trees used to root the tree of life using two universal paralogs that  
208 have been previously used for this purpose: Elongation factors and catalytic and non-  
209 catalytic subunits of the rotary ATPase. We begin with the Elongation factor phylogeny.  
210 Elongation factor EF-Tu/EF-2 delivers aminoacyl-tRNAs to the A-site of the ribosome while  
211 the Elongation Factor EF-G/EF-1A catalyses the translocation of the peptidyl-tRNA (Miller,  
212 1972). Both paralogs are conserved across the tree of life, making them an ideal candidate  
213 for paralog rooting (Baldauf et al., 1996; Philippe and Forterre, 1999; Gouy et al., 2015). In  
214 all previous attempts to root the tree of life using EF-G and EF-Tu, the branch separating the  
215 paralogs is extremely long and potentially completely saturated, which implies that the  
216 position of the root within each paralog might be determined entirely by the substitution  
217 model and not by any synapomorphies between the paralogs. In addition, the two paralogs  
218 do not root each other consistently increasing the uncertainty.  
219

220 To test if our new matrix can help solve this problem, we first assembled a dataset of 1076  
221 homologs of EF-Tu and EF-G. In an amino acid-based ML tree we also recover a very long  
222 branch (Branch length (BL) = 3.284) between the two paralogs albeit still separating the  
223 bacteria and archaea (Figure 2A). In line with previous phylogenies, this tree recovers  
224 different roots for the tree of life in the two paralogs: between bacteria and archaea plus  
225 eukaryotes, and between archaea and bacteria plus eukaryotes (Figure 2B). We then  
226 extracted 3Di sequences from 1076 AlphaFold predictions using FoldSeek (see methods)  
227 and utilized our new Q.3Di.AF Q-matrix as the substitution model, to estimate a new tree of  
228 the EF-G and EF-tu paralogs. This recovered a phylogenetic tree with the length of the  
229 branch separating the paralogs far below 1 (0.186). Crucially, the root position is now  
230 consistent in both the paralogs and indicates a root between archaea and bacteria for life  
231 (Figure 2C). The archaea in both paralogs remain paraphyletic, which is consistent with the  
232 two-domain tree of life.

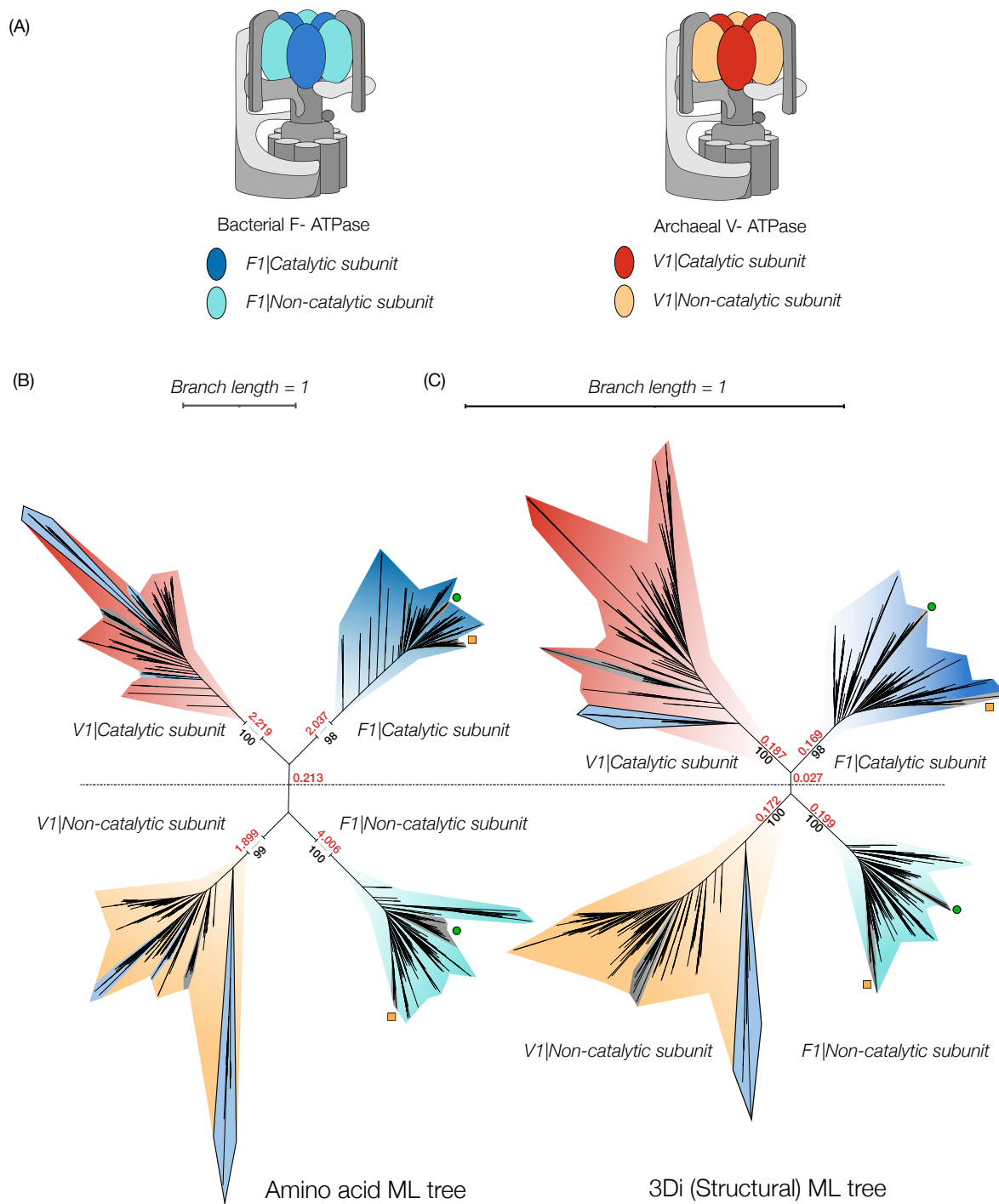


233  
234 Figure 2: (A) A schematic representation of paralog rooting. Three possible root positions are shown with the  
235 “true” root depicted with a green star and two other possible roots with circles. In the scenario where  
236 paralogous rooting is successful both paralog subtrees reciprocally root each other (right). Other possible  
237 scenarios are also shown where the paralog subtrees are ambiguously rooted (left). (B) Amino acid ML tree  
238 containing 1076 EF-tu and EF-G homologs from eukaryotes, bacteria and archaea. The mitochondrial and  
239 plastid encoded copies are not included. Note that the branch separating the EF-tu and EF-G is broken for  
240 illustration. (C) 3Di structural ML tree estimated 3Di sequences and the Q.3Di.AF model from the predicted  
241 AlphaFold structures of 1069 EF-tu and EF-G homologs. In both cases blue, red and grey clades represent  
242 bacteria, archaea and eukaryotes respectively. Numbers in red, black indicate branch lengths and ultrafast  
243 bootstrap supports respectively.

244  
245 Another universally conserved paralogous gene family used to root the tree of life are the  
246 catalytic and non-catalytic subunits of the rotary ATPase. The head group of the rotary  
247 ATPase is a hexamer consisting of two subunits, only one of which is catalytic (Figure 3A).  
248 The bacterial and mitochondrial ATPases are called the F<sub>0</sub>F<sub>1</sub>-ATPases, and their subunits  
249 are called F1-alpha and F1-beta for the non-catalytic and catalytic subunits respectively  
250 (Grüber et al., 2001). The archaeal ATPase is called the V-ATPase and shares a similar  
251 architecture with a non-catalytic and a catalytic subunit in its headgroup (Figure 3A). Owing  
252 to the endosymbiotic event between archaea and bacteria at eukaryogenesis, the  
253 eukaryotes and archaea also share this ATPase which in eukaryotes is in the vacuole, where  
254 it functions to acidify lysosomes (Gogarten et al., 1989). The archaeal/eukaryotic subunits

255 are named V1-beta and V1-alpha for the non-catalytic and catalytic subunits respectively  
256 (Grüber et al., 2001; Cross and Müller 2004). A recent analysis on rooting the ToL using the  
257 ATPase subunits (Mahendrarajah et al., 2023) recovers a tree that separates the four major  
258 subunits with extremely long basal branches (Figure 3B). This tree is consistent with the  
259 idea that the catalytic and non-catalytic subunits originated before the divergence of  
260 archaea and bacteria, and roots the tree of life between these two domains. The same study  
261 also identified an early transfer of the archaeal non-catalytic subunit into bacteria,  
262 however, the catalytic counterpart to this transfer was not recovered in the catalytic sub-  
263 tree suggesting multiple transfer events (Figure 3B).

264  
265 As before, we predicted AlphaFold structures for all 1520 sequences and extracted the 3Di  
266 sequences using FoldSeek and calculated a 3Di (structural) ML tree with the Q.3Di.AF as  
267 the substitution model. While the tree in this case looks remarkably like the amino acid ML  
268 tree, the 3Di structural ML tree has significantly shorter branches (Figure 3C). This new  
269 topology also reconfirms the root of ToL as between the archaea and bacteria.  
270 Furthermore, in the 3Di tree the early transfer of the archaeal ATPase subunits is recovered  
271 basal in both catalytic and the non-catalytic subtrees suggesting a single early transfer from  
272 archaea to bacteria. Together with the Elongation factors, our results bolster support for the  
273 two-domain tree of life with the eukaryotes branching within archaea. In both these cases  
274 it is evident that structural phylogenetics can resolve deep phylogenies and recover  
275 consistent groupings within the paralogs despite large divergences in amino acid  
276 sequences.



277  
278

279 *Figure 3: (A) A schematic representation of the bacterial and archaeal ATPase highlighting the subunits under*  
 280 *investigation. They are represented using the same colours in the phylogenetic trees. (B) Amino acid ML tree*  
 281 *of 1520 sequences across the ToL reproduced from Mahendarajah et al., 2023 of the catalytic and non-*  
 282 *catalytic subunits of bacterial, archaeal, and eukaryotic rotary ATPase. The early branching transfer from*  
 283 *bacteria and archaea in the non-catalytic V1 clade is highlighted in blue with a black outline. The*  
 284 *corresponding clade in the V1 catalytic clade branches deep inside of the archaeal sequences and is*  
 285 *highlighted similarly. (C) 3Di structural tree estimated using the Q.3Di.AF model. Sequences assigned to the*  
 286 *early transfer from the archaeal clade to bacteria are highlight as in (B), but now this transfer is inferred for*  
 287 *both the catalytic and non-catalytic subunits. Numbers in red, black indicate branch lengths and ultrafast*  
 288 *bootstrap supports respectively. In both cases grey clades represent eukaryotes. The green circles and orange*  
 289 *squares indicate cyanobacterial and proteobacterial contributions in eukaryotes representing the plastid and*  
 290 *mitochondrial ATPases.*

291

292 *Evolution of photosystems RCI and RCII*

293

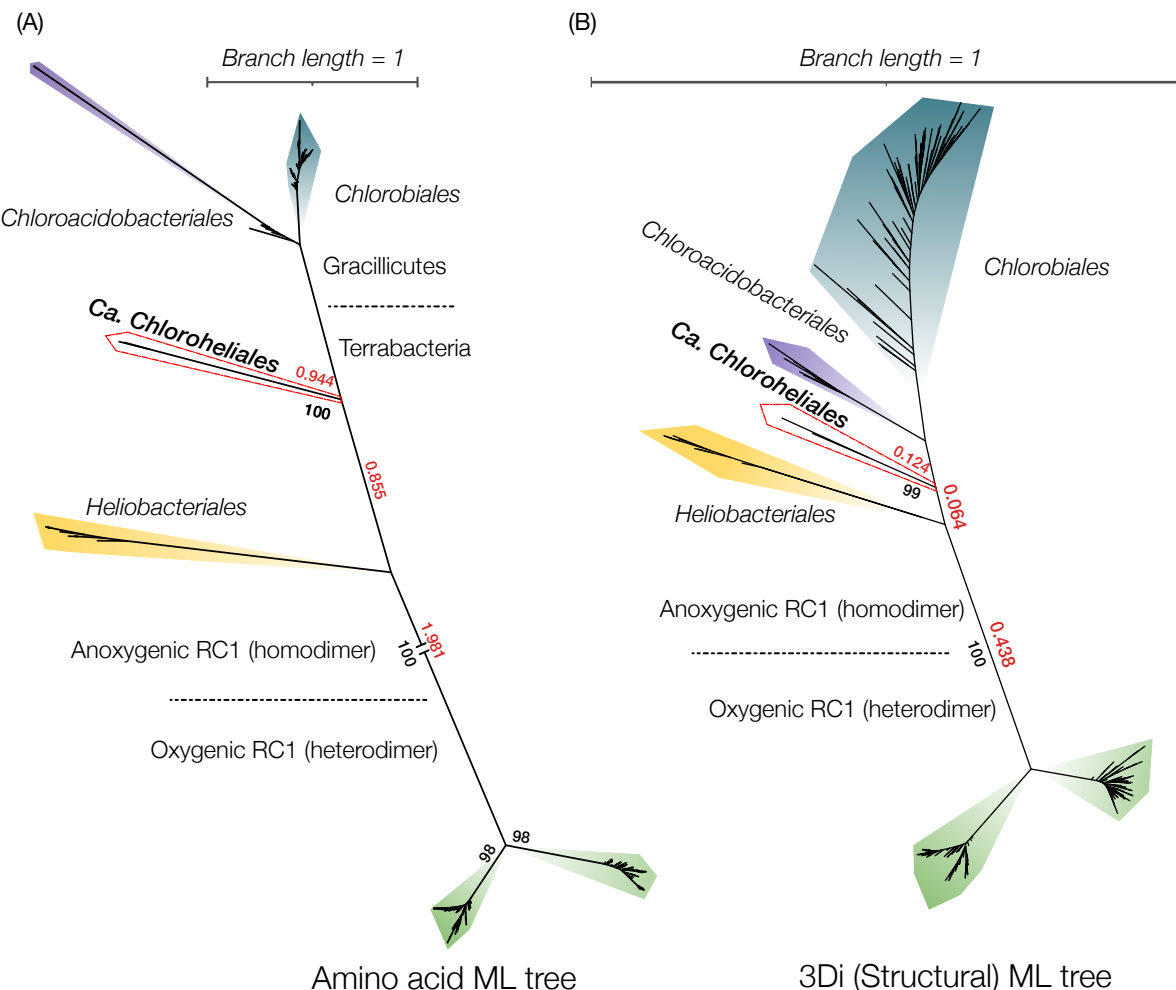
294 The issue of saturation is not exclusive to tree-of-life problems but to all evolutionarily  
295 divergent proteins that share remote homology in sequence. The origin of oxygenic  
296 photosynthesis is another event that impacted the overall geochemistry of the planet and  
297 has been the subject of contentious debate. Photosynthesis can be classified into two  
298 major types: anoxygenic photosynthesis, which uses either reaction centre II (RCII) or  
299 reaction centre I (RCI), but never both together and oxygenic photosynthesis which uses  
300 both reaction centres I and II (RCI and RCII) coupled to a water splitting reaction that leads  
301 to the formation of oxygen (Hohmann-Marriott and Blankenship, 2011). One set of theories  
302 suggests that anoxygenic photosynthesis evolved first and later developed into oxygenic  
303 photosynthesis (Martin et al., 2018). An alternative view favours oxygenic photosynthesis to  
304 have evolved first, with anoxygenic phototrophs having lost either RCI or RCII. One piece of  
305 evidence for the latter view is the lack of any bacterial group that harbours the anoxic  
306 versions of both RCI and RCII, which is thought to be a necessary precursor to oxygenic  
307 photosynthesis (Sánchez-Baracaldo and Cardona, 2020). Until recently, members of the  
308 *chloroflexota* phylum have only been known to harbour anoxic RCII. This changed when a  
309 *chloroflexota* group, *Ca. Chloroheliales*, was identified that contains RCI (Tsuji et al.,  
310 2024). This still falls short of proving that anoxic RCI and RCII have existed together in the  
311 same genome however, one possible interpretation of these data is that an ancestral  
312 *Chloroflexus* might have contained both, leading to differential losses in extant lineages of  
313 *Chloroflexi*. This would support the idea that anoxic photosynthesis may have come first, if  
314 these photosystems are close relatives of the photosystems that were eventually  
315 transferred into cyanobacteria

316

317 The phylogenetic tree based on amino acids of RCI containing *Chloroflexi* does not place  
318 their RCI sequences as close relatives to those of cyanobacteria (4A, re-inferred for this  
319 study). But this tree suffers from extremely long branches, and we wondered whether this  
320 placement is the result of long branch attraction. We therefore set out to re-infer this tree  
321 using 3Di characters and our structural substitution matrix (Figure 4B). This shortened all  
322 relevant internal branches to lengths well below one but yielded the same topology as the  
323 amino acid tree. This confirms the authors' original inferences and leaves the evolution of  
324 oxygenic photosynthesis an unsolved problem for now.

325

326



327  
328 Figure 4: (A) Amino acid ML tree of 321 RC1 protein sequences. Note that long branches are broken as  
329 indicated for illustration. (B) 3Di structural ML tree of 297 3Di sequences from AlphaFold structures using the  
330 Q.3Di.AF model. Numbers in red, black indicate branch lengths and ultrafast bootstrap supports respectively.  
331  
332

333 Our work in this manuscript and that of others (Moi et al., 2023; Puente-Lelievre et al., 2024)  
334 clearly points to the utility of structural phylogenetics in cases where structures can be  
335 predicted reliably and with one possible structure per sequence. There are several practical  
336 and conceptual caveats that come with using this method, which we will briefly elaborate  
337 on. We present these caveats in the spirit of critical optimism about the utility and impact  
338 of this new method.  
339

#### 340 *Prediction accuracy of LLMs*

341  
342 Structural phylogenies can only ever be as good as the predicted models that are used to  
343 derive 3Di sequences. Predicting large numbers of sequences with AlphaFold is  
344 computationally costly and potentially prohibitive for many interested users. Using bilingual  
345 Protein LLMs like ProtT5 may seem like an obvious solution, because it removes the  
346 computationally expensive requirement of predicting the AF structures of a large number of  
347 protein clusters not only in the Q-matrix estimation, but also for tree inference of single  
348 protein families with a lot of members. Encouragingly, the Q-matrix estimated from 3Di

349 sequences derived from AlphaFold structures (Q.3di.AF) is very similar to the one from  
350 PFAM clusters translated using ProtT5 (Q.3Di.LLM) despite their low accuracy compared to  
351 AlphaFold predictions (Figure 1C, 1D, Supplementary Figure 1). This could be due to the fact  
352 that the LLM has issues when dealing with long repeated stretches which in some cases  
353 leads to possible register shifts of structural motifs (Supplementary Figure 2). These register  
354 shifts can be dealt with during a 3Di sequence alignment using the 3Di scoring matrix, which  
355 we did not perform for our pairwise identity calculations (as the two sequences are the  
356 same length). It is also possible that prediction errors average out when inferring a Q-matrix  
357 for thousands of protein families, even if there are substantial errors in the alignments of  
358 any one family. It is clear, however, that ProtT5 translations are not reliable for inferring  
359 individual trees. We tested this by using ProtT5 derived 3Di alignments for the three protein  
360 families we investigated here. In two out of three cases we recovered phylogenies that  
361 either were biologically improbable (Supplementary Figure 4) and/or erroneous with non-  
362 sensical topologies (Supplementary Figure 5). Most of these issues stem from the faulty  
363 prediction of 3Di sequences. While we did not observe this problem here when using  
364 AlphaFold structures, we expect similar issues when using structures that are not  
365 confidently predicted by AlphaFold. For now, reliable tree inference only seems possible  
366 using AlphaFold generated structures and therefore comes with a significant  
367 computational overhead. Better language and structure prediction models are certain to be  
368 available in the future and they should make structural phylogenetics more widely  
369 accessible.

370

### 371 *Fold-switching and conformational variability*

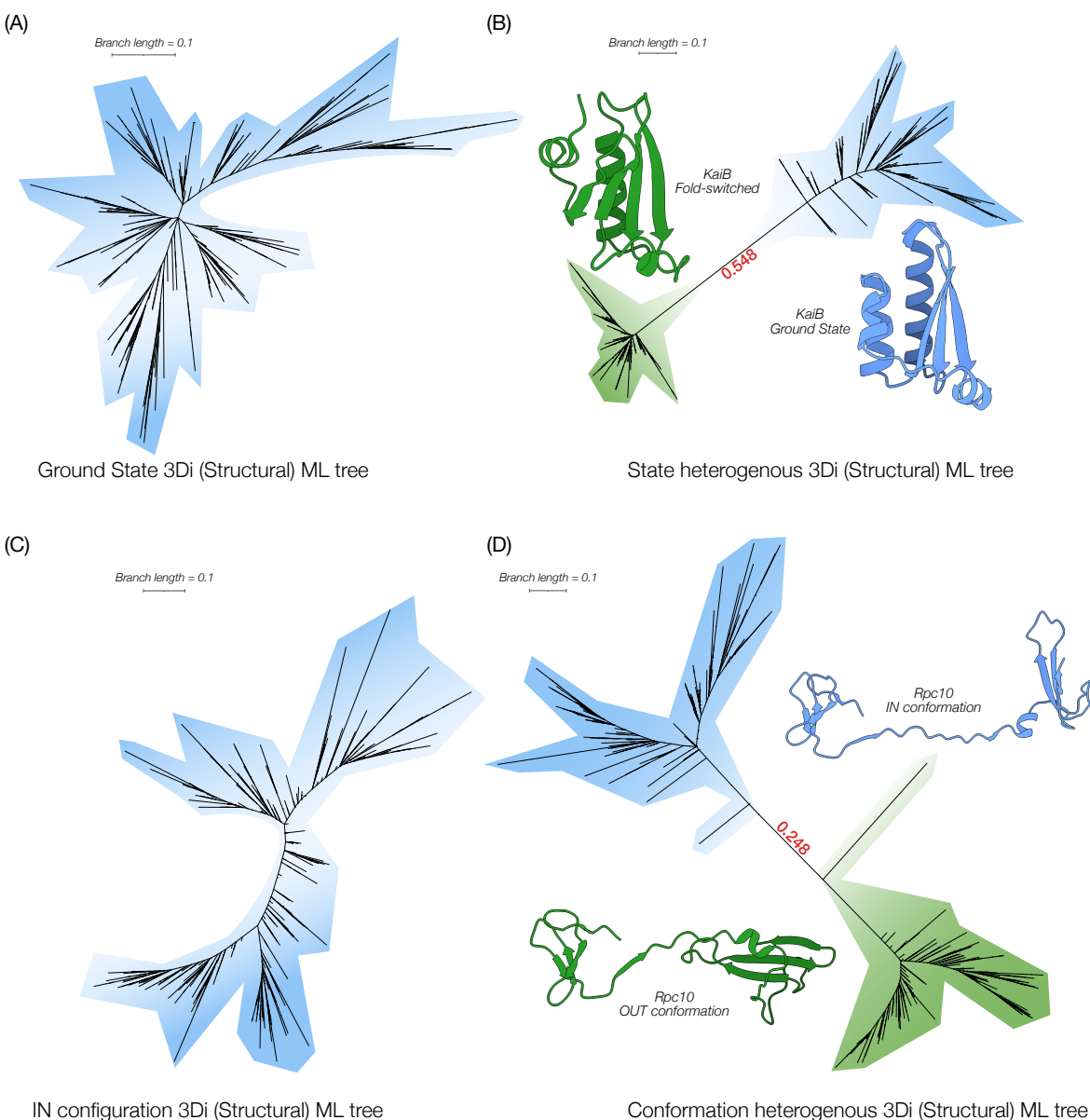
372

373 Many proteins undergo conformational changes and some even switch their folds entirely  
374 as part of their functions (Chang et al., 2015). Previous analyses using AlphaFold suggests  
375 that it can sometimes predict structures in different conformations despite having a strong  
376 bias towards one dominant conformation (Chakravarty and Porter 2022; Sala et al., 2023;  
377 Wayment-Steele et al., 2023). Since this can lead to different 3Di sequences for the same  
378 protein, depending on which conformation it is predicted in, we wondered if this could lead  
379 to spurious grouping according to conformation rather than genealogical relationships on  
380 3Di phylogenies. We examined two proteins for this purpose. One is KaiB, which is known  
381 to fold-switch as part of its catalytic cycle, involving a drastic change of a helix to a beta-  
382 sheet (Chang et al., 2015; Zhang et al., 2023). The other is the RNA Polymerase III subunit  
383 Rpc10, which undergoes a conformational change during its function in gene transcription  
384 (Girbig et al., 2021).

385

386 To test how much this issue can affect 3Di trees, we constructed a worst-case scenario for  
387 both proteins. In both cases, we modelled each sequence on the two distinct  
388 conformations using homology modelling and inferred their 3Di sequences using FoldSeek.  
389 For tree inference, we then randomly chose the 3Di sequence of one of the two possible  
390 conformations for each protein, such that approximately half our sequences were  
391 predicted in one conformation, and the other half in the other conformation. For both KaiB  
392 and Rpc10 we found that the phylogenetic tree splits the two conformational states with  
393 long branches (Figure 4B, 4D) as opposed to a 3Di structural tree which was inferred from  
394 3Di sequences reflecting a single conformation (Figure 4A, 4C). This highlights a severe  
395 limitation of structural phylogenetics where the presence of multiple predicted

396 conformations can generate spurious branches and relationships. Here we concocted an  
397 extreme case by forcing sequences randomly into distinct conformations. However, in  
398 cases where only a small minority of proteins within the analyses share a different  
399 conformation, these artefacts can lead to false conclusions. It is therefore very important  
400 to assess the conformational homogeneity of the predicted sequences before inferring a  
401 3Di tree.



402  
403 Figure 5: (A) 3Di structural ML tree constructed from KaiB proteins modelled in the ground state.  
404 (B) 3Di structural ML tree constructed from approximately 50% of the KaiB proteins modelled in the ground state  
405 (blue) and the other 50% modelled in the fold switched state (green). (C) 3Di structural ML tree constructed  
406 from RPC10 proteins modelled in the IN conformation (D) 3Di structural ML tree constructed from  
407 approximately 50% of the RPC10 proteins modelled in the OUT conformation (blue) and the other 50%  
408 modelled in the IN conformation (green). In both cases the distinct conformations form monophyletic groups  
409 in contrast to their placements in (A) and (C) respectively.  
410

411 *Site-independence in structural alignments*  
412

413 One of the main assumptions of maximum likelihood is site independence, which allows  
414 the likelihood to be computed independently for all sites in the alignment (Liò and Goldman  
415 1998). It has been obvious for a long time that this is not a realistic assumption. Epistasis  
416 between amino acids is a well demonstrated phenomenon and quite extensive among  
417 proteins (Starr and Thornton 2016). This violates the site-independence assumption of  
418 maximum likelihood phylogenetics, even though it has been argued that increasing the  
419 number of sites normally associated with a protein sequence or increasing the number of  
420 proteins used for a concatenated alignment averages out the signal in most cases (Starr  
421 and Thornton, 2016; Magee et al., 2021). In the case of the structural phylogenetics and 3Di  
422 alphabet however, this assumption is explicitly violated since each letter corresponds to at  
423 least 6 other amino acid positions in 3D space. It is for example not clear to us that it is even  
424 possible for a single substitution to occur at the level of 3Di characters, because of the  
425 structural dependence between sites. In a sense, structural phylogenetics makes the ugly  
426 truth of model violation explicit in its alphabet. Whether or not this approach becomes  
427 widely accepted in evolutionary biology will depend on investigating the consequences of  
428 this violation, which is beyond the scope of this manuscript.

429

430 *Information loss*

431

432 The 3Di alphabet compresses information that would be present in amino acids. This is the  
433 very reason for its utility in deep phylogenetics, because it overcomes the saturation  
434 problem. But it also makes evolution on short time-scales is harder to resolve using these  
435 models, and relationships at the very tips of 3Di trees probably much less reliable than in  
436 an amino acid or DNA tree (Mutti et al., 2024). A potential solution is to use partitioned  
437 models, in which a tree is inferred from both 3Di and amino acid alignments  
438 simultaneously, using different substitution models for the partitions (Puente-Lelievre et  
439 al., 2024). To make this approach work, however, one would have to allow the structural  
440 partition to also have a different set of branch lengths than the amino acid partition (Lopez  
441 et al., 2002), which the first use of this approach did not yet include (Puente-Lelievre et al.,  
442 2024). Such a heterotachous model presents a difficult optimization problem, which in our  
443 hands leads to impractically long run times on our datasets. Another question is the size of  
444 the alphabet. 3Di uses 20 characters because this allows simple integration with existing  
445 phylogenetic software. It is not yet clear that whether this is even close to the optimal  
446 number of characters for structural phylogenetics. Larger alphabets could perhaps retain  
447 more short-term information. They would, however, make the inference of substitution  
448 matrices much harder.

449

450 *Structural phylogenetics and the future of deep history*

451

452 Our work complements and builds on other recent tools that utilise the 3Di alphabet for  
453 structural phylogenetics (Moi et al., 2023; Puente-Lelievre et al., 2024). Our structural Q-  
454 matrices should make it much easier to infer structure-based trees for anyone familiar with  
455 maximum likelihood phylogenetics. Newly developed online tools for the generation of 3Di  
456 alignments should further lower the bar for adoption (Gilchrist et al., 2024). As with every  
457 new method, it is difficult to know exactly what impact structural phylogenetics will have.  
458 For now, we see its main utility in solving difficult rooting problems involving distant  
459 outgroups that amino acid phylogenies cannot solve with any degree of confidence. This

460 will help polarize the direction of evolutionary change in the emergence of many important  
461 functions. Better resolved deep protein phylogenies will also improve our reconstructions  
462 of the gene content of ancient organisms (The Last Universal Common Ancestor, the Last  
463 Eukaryotic Common Ancestor, and the Last Archaeal Common Ancestor, for example).

464  
465 For now, these methods will not be useful for ancestral sequence reconstruction, because  
466 3Di sequences cannot be back translated into a unique amino acid sequence (Heinzinger  
467 et al., 2023). Even though our matrix allows us to infer 3Di sequences at internal nodes of  
468 structural phylogenies, it is at present not possible to then turn these reconstructed 3Di  
469 sequences into resurrected proteins composed of amino acids. It may, however, be  
470 possible to restrict a set of plausible amino acid reconstructions at one particular node on  
471 an amino acid phylogeny to a subset that agrees with the reconstructed ancestral 3Di  
472 sequence at the corresponding node on a structural phylogeny.

473  
474 The true impact of viewing the past through the glacial change in the structure of proteins  
475 will only emerge when this method is robustly tested and becomes widely adopted in  
476 evolutionary biology. We hope the matrix inferred here will be a first step in this process.

477  
478 **Methods**

479  
480 *Datasets for QMaker*

481 The SwissProt AlphaFold database (<https://alphafold.ebi.ac.uk/download>) was  
482 downloaded and then clustered with FoldSeek (<https://github.com/steineggerlab/foldseek>)  
483 easy-cluster with default settings and a coverage of 80%. This yielded 1660 clusters which  
484 contained at least 50 members and a maximum of 2500 members. Databases of PDB  
485 structures were then created and 3Di sequences were subsequently extracted from these  
486 1660 clusters using FoldSeek as previously described. The PFAM sets were taken from  
487 Minh et al., 2021 which contained 6655 protein families used for training the Q-matrix and  
488 a further 6653 families were used for testing. In the case of PFAM families the amino acid  
489 FASTA files were directly translated to the 3Di alphabet using the scripts provided by  
490 Heinzinger et al., 2023 (<https://github.com/mheinzinger/ProstT5>).

491  
492 *Q-matrix estimation*

493 Both the AF-db and PFAM-db sets of 3Di sequences were aligned using *ginsi* method within  
494 Mafft (v7.515) and the 3Di scoring matrix from FoldSeek using the *--aamatrix* flag  
495 implemented within mafft. The 3Di MSAs thus generated were then used in the QMaker  
496 routine as described in Minh et al., 2021 (<http://www.iqtree.org/doc/Estimating-amino-acid-substitution-models>). Briefly, for each MSA the best fit substitution model was  
497 initialised with GTR20 along with the best RHAS model to account for rate-heterogeneity  
498 using ModelFinder (Kalyaanamoorthy et al., 2017). In the Next step we estimate a joint  
499 reversible Q-matrix for all the 3Di MSAs as described.

500  
501  
502 *Individual Protein/3Di sequences and Phylogenetic tree reconstructions*

503 Elongation factors and Reaction Centre I homologs were identified using BLAST against the  
504 NCBI non-redundant (*nr*) database, and then filtered with a minimum similarity threshold  
505 of 50% and an e-value cutoff of 1E-5. For the ATPase phylogeny was exactly reproduced  
506 from Mahendarajah et al., 2023 and the same sequences used for the 3Di sequences. The

507 amino acid sequences were aligned using *linsi* and then subsequently trimmed using TrimAl  
508 (v1.4) (Capella-Gutiérrez et al., 2009) with the *-automated1* setting. Trimmed amino acid  
509 alignments were then used for maximum likelihood tree estimation using IQ-tree with the  
510 best-fit model suggested by ModelFinder. 3Di sequences for individual proteins trees were  
511 extracted from PDB files from individual AlphaFold (v2.2.0) predictions. The best ranked  
512 AlphaFold models were used to create a database using FoldSeek which allowed us to  
513 extract 3Di sequences from the PDB structures. For 3Di sequences translated from ProtT5,  
514 the model was queried as described in Heinzinger et al., 2023 using amino acid sequences  
515 as input. All 3Di sequences were aligned with Mafft (*ginsi*) using the *--aamatrix* option  
516 specifying the 3Di scoring matrix provided by van Kempen et al., as part of FoldSeek. 3Di  
517 MSAs were then used to estimate the structural ML tree as described above. For individual  
518 3Di tree reconstructions IQ-tree (v2.3.0) was used to identify the best-fit model (Q.3Di.AF,  
519 Q.3Di.LLM or GTR20) according to AICc, along with rate-heterogeneity using ModelFinder.  
520 Both amino acid and 3Di trees were estimated with 10000 Ultrafast bootstraps (-bb) and  
521 10000 iterations for SH-test (-alrt).

522

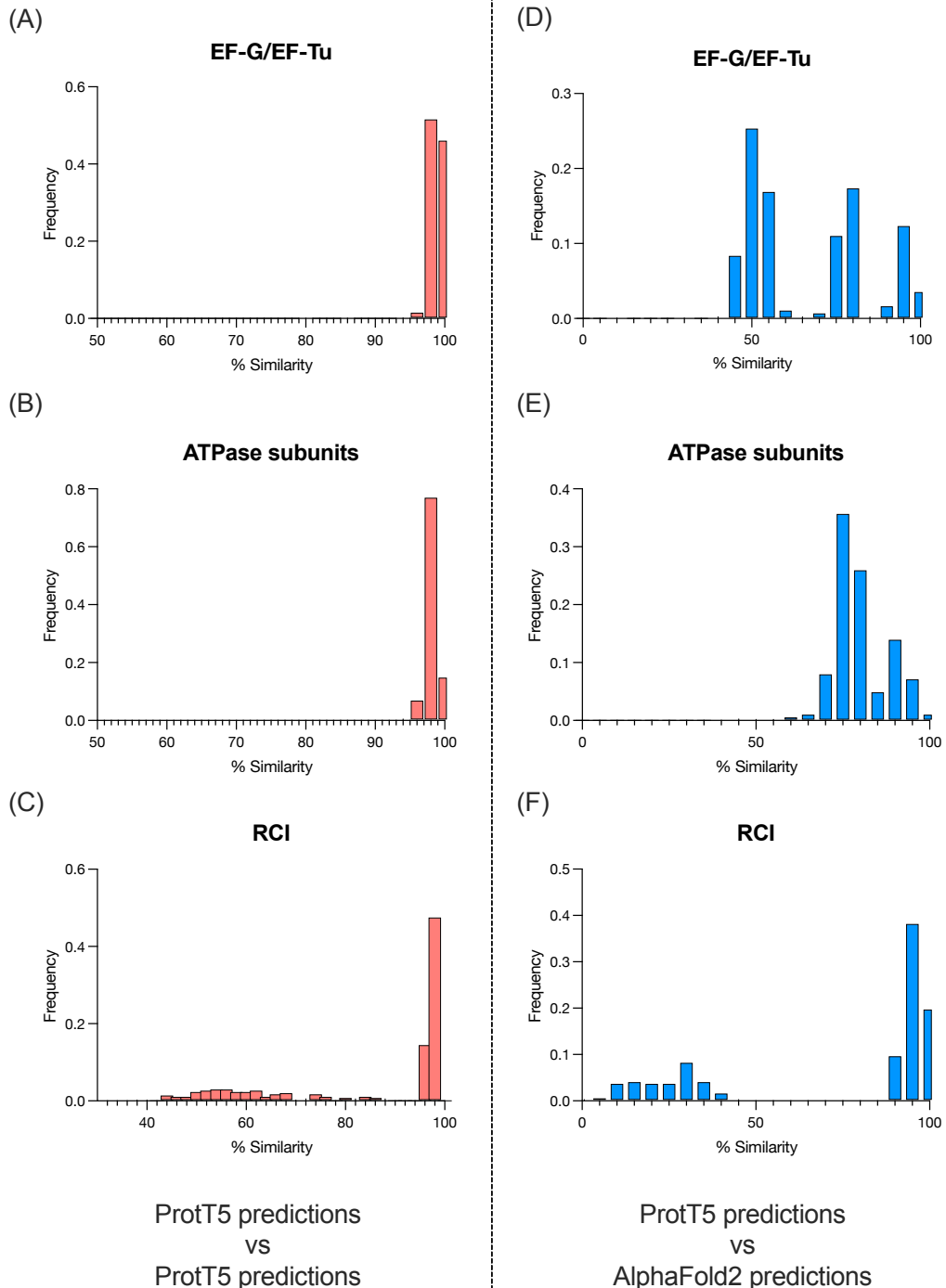
### 523 *Homology Modelling*

524 For the KaiB and RPC10 proteins homologs were identified via BLAST as described above.  
525 Then PDB structures or AlphaFold structures of the two conformations in question were  
526 used as a template in SWISS-MODEL (Waterhouse et al., 2018). KaiB was modelled using  
527 the PDB structure 2QKE in the ground state and 5JYT in the fold-switched state from  
528 *Thermosynechococcus elongatus*. The RPC10 was homology modelled on the PdB  
529 structure 7AE1 in the OUT conformation and 7AE3 in the IN conformation as described in  
530 (Girbig et al., 2021). 3Di sequences were extracted from both sets of states/conformations  
531 and then randomly sampled to generate a set composed approximately 50% of 3Di  
532 sequences from PDB of KaiB and RPC10 in one of the two states/conformation. ML trees  
533 were then estimated using these proteins sequences as described above.

534

535

### 536 **Supplementary Figure Legends**

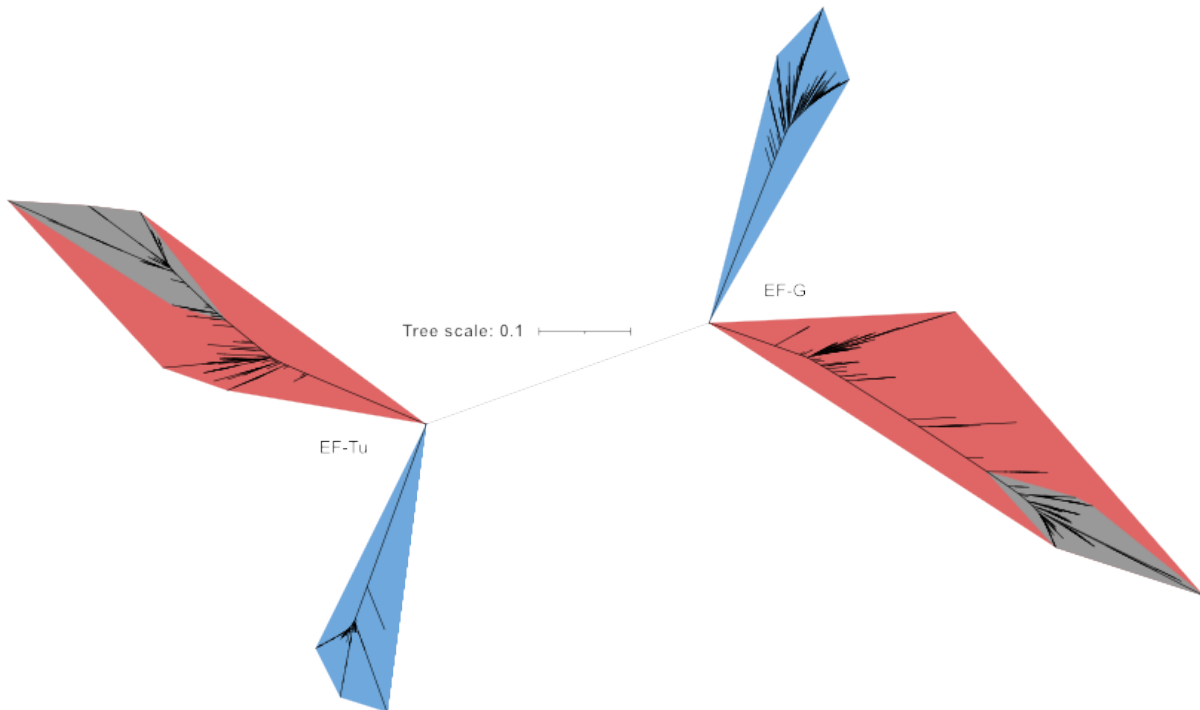


537

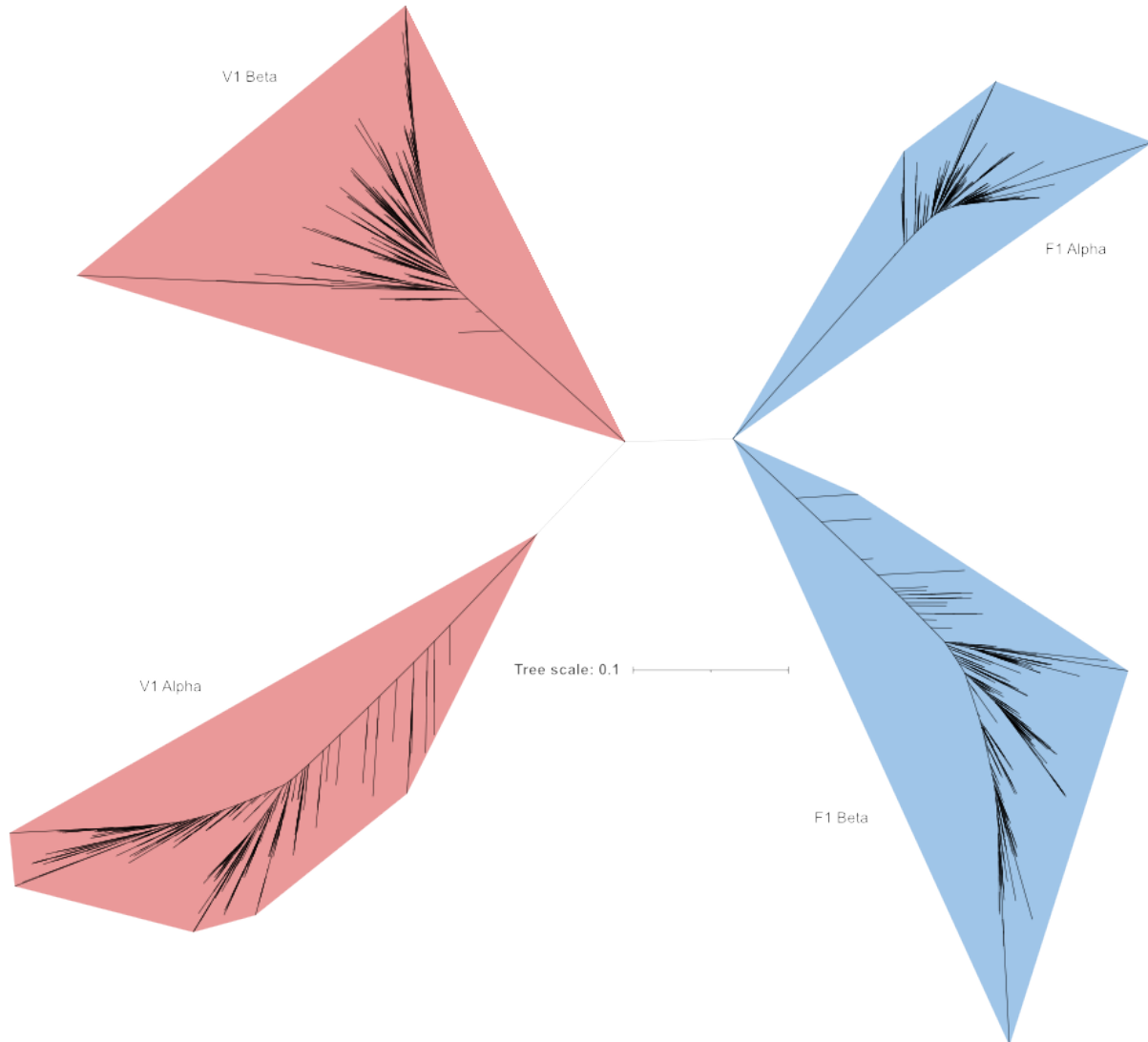
538 **Supplementary Figure 1:** (A-C) Average Percentage similarity between 10 independent  
539 rounds of 3Di translations using the ProtT5 model for Elongation factors, ATPase subunits  
540 and the Reaction Centre I proteins respectively. (D-F) Percentage similarity between 3Di  
541 translation using the ProtT5 model and 3Di sequences extracted from AlphaFold predicted  
542 structures for Elongation factors, ATPase subunits and the Reaction Centre I proteins  
543 respectively. In all cases percentage similarities were calculated based on the BLOSUM  
544 style 3Di scoring matrix on unaligned sequences. Results show that the ProtT5 model is  
545 more precise than it is accurate when compared to AlphaFold predictions in all the three  
546 cases tested

547

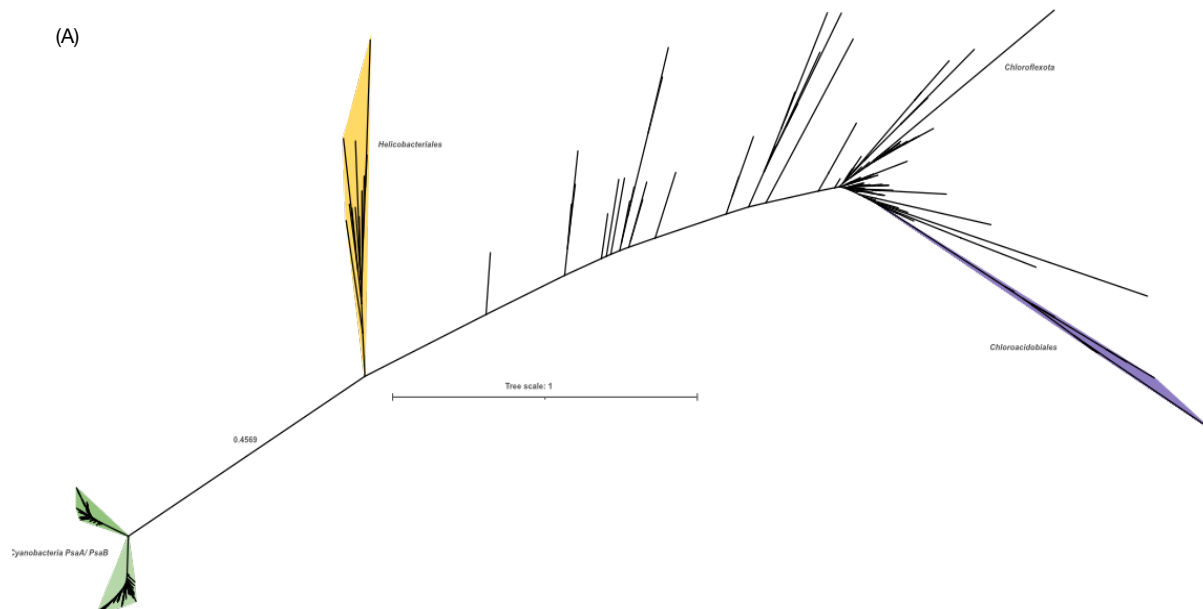




559  
560 **Supplementary Figure 3:** (A) 3Di (structural) ML tree on 3Di translations using ProtT5 of  
561 Elongation factor proteins. Red, Blue, and Grey represent Archaeal, Bacterial, and  
562 Eukaryotic groups respectively. This particular tree recovers the two-domain topology for  
563 the tree of life albeit consistent with the 3Di (structural) ML tree estimated from 3Di  
564 sequences extracted from AlphaFold structures.



565  
566 **Supplementary Figure 4:** (A) 3Di (structural) ML tree on 3Di translations using ProtT5 of  
567 ATPase subunits. Red Blue, and Grey represent Archaeal, Bacterial, and Eukaryotic groups  
568 respectively. V1 Alpha and F1 Beta are the catalytic subunits while V1 Beta and F1 Alpha  
569 are non-catalytic. This tree recovers a root for the tree of life between archaea and bacteria.  
570 It does, however, groups the respective catalytic and non-catalytic subunits of bacteria  
571 together, as well as the catalytic and non-catalytic subunits of archaea. This would require  
572 an independent loss of catalytic activities in one of the subunits in both the groups. This is  
573 inconsistent with currently established theories on the origin of the rotary ATPase. For  
574 comparison, our structural tree derived from AlphaFold predictions (Figure 3C) groups  
575 archaeal and bacterial catalytic subunits as one monophyletic group and the non-catalytic  
576 subunits as another.



577  
578 **Supplementary Figure 5: (A)** 3Di (structural) ML tree on 3Di translations using ProtT5 of  
579 ATPase subunits. This particular tree is highly inconsistent and does not recover the split  
580 between chlorobiales and chloroacidobiales. This is also evident from the particularly low  
581 similarities between the 3Di translations using ProtT5 and the 3Di sequences extracted  
582 from AlphaFold structures. Such cases highlight the importance of the quality of the  
583 structure predictions.

584

#### 585 **Author Contributions**

586 SGG and GKAH conceptualized, designed and wrote the manuscript. SGG performed the  
587 computations

588

#### 589 **Acknowledgments and Funding**

590 We would like to thank Mathias Girbrig for suggesting RPC10 for studying the impact of  
591 conformational heterogeneity. The study was funded by the Human Frontiers Science  
592 Program Grant (RGP0028) awarded to GKAH.

593

#### 594 **Data availability**

595 All datasets, trees and alignments are available at

596 <https://edmond.mpg.de/privateurl.xhtml?token=624d9e21-f33d-408b-8a81-93d9ad020426> for review and will be made fully public on publication.

598

#### 599 **References**

600

601 Balaji S, Srinivasan N. 2001. Use of a database of structural alignments and phylogenetic  
602 trees in investigating the relationship between sequence and structural variability among  
603 homologous proteins. *Protein Eng.* 14:219–226.

604 Balaji S, Sujatha S, Kumar SSC, Srinivasan N. 2001. PALI—a database of Phylogeny and  
605 ALignment of homologous protein structures. *Nucleic Acids Res.* 29:61–65.

606 Baldauf SL, Palmer JD, Doolittle WF. 1996. The root of the universal tree and the origin  
607 of eukaryotes based on elongation factor phylogeny. *Proc. Natl. Acad. Sci.* 93:7749–  
608 7754.

609 Brown JR, Doolittle WF. 1995. Root of the universal tree of life based on ancient  
610 aminoacyl-tRNA synthetase gene duplications. *Proc. Natl. Acad. Sci.* 92:2441–2445.

611 Capella-Gutiérrez S, Silla-Martínez JM, Gabaldón T. 2009. trimAl: a tool for automated  
612 alignment trimming in large-scale phylogenetic analyses. *Bioinformatics* 25:1972–  
613 1973.

614 Chakravarty D, Porter LL. 2022. AlphaFold2 fails to predict protein fold switching.  
615 *Protein Sci.* 31:e4353.

616 Chang Y-G, Cohen SE, Phong C, Myers WK, Kim Y-I, Tseng R, Lin J, Zhang L, Boyd JS, Lee  
617 Y, et al. 2015. A protein fold switch joins the circadian oscillator to clock output in  
618 cyanobacteria. *Science* 349:324–328.

619 Cross RL, Müller V. 2004. The evolution of A-, F-, and V-type ATP synthases and  
620 ATPases: reversals in function and changes in the H+/ATP coupling ratio. *FEBS Lett.*  
621 576:1–4.

622 Farris JS. 1970. Methods for computing wagner trees. *Syst. Biol.* 19:83–92.

623 Felsenstein J. 1981. Evolutionary trees from DNA sequences: A maximum likelihood  
624 approach. *J. Mol. Evol.* 17:368–376.

625 Felsenstein J. 2003 Inferring phylogenies. *Sinauer Associates, Sunderland,*  
626 *Massachusetts.*

627 Fitch WM. 1971. Toward defining the course of evolution: minimum change for a  
628 specific tree topology. *Syst. Zoöl.* 20:406.

629 Gilchrist CLM, Mirdita M, Steinegger M. 2024. Multiple protein structure alignment at  
630 scale with FoldMason. *bioRxiv*:2024.08.01.606130.

631 Girbig M, Misiaszek AD, Vorländer MK, Lafita A, Grötsch H, Baudin F, Bateman A, Müller  
632 CW. 2021. Cryo-EM structures of human RNA polymerase III in its unbound and  
633 transcribing states. *Nat. Struct. Mol. Biol.* 28:210–219.

634 Gogarten JP, Kibak H, Dittrich P, Taiz L, Bowman EJ, Bowman BJ, Manolson MF, Poole  
635 RJ, Date T, Oshima T, et al. 1989. Evolution of the vacuolar H+-ATPase: implications  
636 for the origin of eukaryotes. *Proc. Natl. Acad. Sci. USA.* 17:6661–5.

637 Gouy R, Baurain D, Philippe H. 2015. Rooting the tree of life: the phylogenetic jury is still  
638 out. *Philos. Trans. R. Soc. B: Biol. Sci.* 370:20140329.

639 Grüber G, Wieczorek H, Harvey WR, Müller V. 2001. Structure–function relationships of  
640 A-, F- and V-ATPases. *J. Exp. Biol.* 204:2597–2605.

641 Heinzinger M, Weissenow K, Sanchez JG, Henkel A, Steinegger M, Rost B. 2023. ProstT5:  
642 bilingual language model for protein sequence and structure.  
643 *bioRxiv*:2023.07.23.550085.

644 Hohmann-Marriott MF, Blankenship RE. 2011. Evolution of photosynthesis. *Plant Biol.*  
645 62:515–548.

646 Iwabe N, Kuma K, Hasegawa M, Osawa S, Miyata T. 1989. Evolutionary relationship of  
647 archaebacteria, eubacteria, and eukaryotes inferred from phylogenetic trees of  
648 duplicated genes. *Proc. Natl. Acad. Sci.* 86:9355–9359.

649 Johnson MS, Šali A, Blundell TL. 1990. [42] Phylogenetic relationships from three-  
650 dimensional protein structures. *Methods Enzym.* 183:670–690.

651 Johnson MS, Sutcliffe MJ, Blundell TL. 1990. Molecular anatomy: Phyletic relationships  
652 derived from three-dimensional structures of proteins. *J. Mol. Evol.* 30:43–59.

653 Jumper J, Evans R, Pritzel A, Green T, Figurnov M, Ronneberger O, Tunyasuvunakool K,  
654 Bates R, Žídek A, Potapenko A, et al. 2021. Highly accurate protein structure  
655 prediction with AlphaFold. *Nature* 596:583–589.

656 Kalyaanamoorthy S, Minh BQ, Wong TKF, Haeseler A von, Jermiin LS. 2017.  
657 ModelFinder: fast model selection for accurate phylogenetic estimates. *Nat.*  
658 *Methods* 14:587–589.

659 Kempen M van, Kim SS, Tumescheit C, Mirdita M, Lee J, Gilchrist CLM, Söding J,  
660 Steinegger M. 2023. Fast and accurate protein structure search with Foldseek. *Nat.*  
661 *Biotechnol.*:1–4.

662 Le SQ, Gascuel O. 2008. An improved general amino acid replacement matrix. *Mol.*  
663 *Biol. Evol.* 25:1307–1320.

664 Liò P, Goldman N. 1998. Models of molecular evolution and phylogeny. *Genome Res.*  
665 8:1233–1244.

666 Lopez P, Casane D, Philippe H. 2002. Heterotachy, an important process of protein  
667 evolution. *Mol. Biol. Evol.* 19:1–7.

668 Magee AF, Hilton SK, DeWitt WS. 2021. Robustness of phylogenetic inference to model  
669 misspecification caused by pairwise epistasis. *Mol. Biol. Evol.* 38:4603–4615.

670 Mahendarajah TA, Moody ERR, Schrempf D, Szánthó LL, Dombrowski N, Davín AA,  
671 Pisani D, Donoghue PCJ, Szöllősi GJ, Williams TA, et al. 2023. ATP synthase evolution  
672 on a cross-braced dated tree of life. *Nat. Commun.* 14:7456.

673 Martin WF, Bryant DA, Beatty JT. 2018. A physiological perspective on the origin and  
674 evolution of photosynthesis. *FEMS Microbiol. Rev.* 2:205-231

675 Mau B, Newton MA. 1997. Phylogenetic inference for binary data on dendograms using  
676 markov chain monte carlo. *J. Comput. Graph. Stat.* 6:122–131.

677 Mihaescu R, Levy D, Pachter L. 2009. Why neighbor-joining works. *Algorithmica* 54:1–  
678 24.

679 Miller DL. 1972. Elongation factors EF Tu and EF G interact at related sites on  
680 ribosomes. *Proc. Natl. Acad. Sci. USA.* 3:752-5.

681 Minh BQ, Dang CC, Vinh LS, Lanfear R. 2021. QMaker: Fast and accurate method to  
682 estimate empirical models of protein evolution. *Syst. Biol.* 70:syab010-.

683 Moi D, Bernard C, Steinegger M, Nevers Y, Langleib M, Dessimoz C. 2023. Structural  
684 phylogenetics unravels the evolutionary diversification of communication systems in  
685 gram-positive bacteria and their viruses. *bioRxiv*:2023.09.19.558401.

686 Mutti G, Ocaña-Pallarés E, Gabaldón T. 2024. Newly developed structure-based  
687 methods do not outperform standard sequence-based methods for large-scale  
688 phylogenomics. *bioRxiv*:2024.08.02.606352

689 Philippe H, Brinkmann H, Lavrov DV, Littlewood DTJ, Manuel M, Wörheide G, Baurain D.  
690 2011. Resolving difficult phylogenetic questions: Why more sequences are not  
691 enough. *PLoS Biol.* 9:e1000602.

692 Philippe H, Forterre P. 1999. The rooting of the universal tree of life is not reliable. *J. Mol.*  
693 *Evol.* 49:509–523.

694 Posada D, Crandall KA. 2021. Felsenstein phylogenetic likelihood. *J. Mol. Evol.* 89:134–  
695 145.

696 Puente-Lelievre C, Malik AJ, Douglas J, Ascher D, Baker M, Allison J, Poole A, Lundin D,  
697 Fullmer M, Bouckert R, et al. 2024. Tertiary-interaction characters enable fast,  
698 model-based structural phylogenetics beyond the twilight zone.  
699 *bioRxiv*:2023.12.12.571181.

700 Rannala B, Yang Z. 1996. Probability distribution of molecular evolutionary trees: A new  
701 method of phylogenetic inference. *J. Mol. Evol.* 43:304–311.

702 Saitou N, Nei M. 1987. The neighbor-joining method: a new method for reconstructing  
703 phylogenetic trees. *Mol. Biol. Evol.* 4:406–425.

704 Sala D, Engelberger F, Mchaourab HS, Meiler J. 2023. Modeling conformational states  
705 of proteins with AlphaFold. *Curr. Opin. Struct. Biol.* 81:102645.

706 Sánchez-Baracaldo, P. and Cardona, T. 2020. On the origin of oxygenic photosynthesis  
707 and cyanobacteria. *New Phytol.* 225: 1440-1446.

708 Starr TN, Thornton JW. 2016. Epistasis in protein evolution. *Protein Sci.* 25:1204–1218.

709 Tsuji JM, Shaw NA, Nagashima S, Venkiteswaran JJ, Schiff SL, Watanabe T, Fukui M,  
710 Hanada S, Tank M, Neufeld JD. 2024. Anoxygenic phototroph of the Chloroflexota  
711 uses a type I reaction centre. *Nature* 627:915–922.

712 Varadi M, Bertoni D, Magana P, Paramval U, Pidruchna I, Radhakrishnan M, Tsenkov M,  
713 Nair S, Mirdita M, Yeo J, et al. 2023. AlphaFold Protein Structure Database in 2024:  
714 providing structure coverage for over 214 million protein sequences. *Nucleic Acids  
715 Res.* 52:D368–D375.

716 Waterhouse A, Bertoni M, Bienert S, Studer G, Tauriello G, Gumienny R, Heer FT, Beer  
717 TAP de, Rempfer C, Bordoli L, et al. 2018. SWISS-MODEL: homology modelling of  
718 protein structures and complexes. *Nucleic Acids Res.* 46:W296–W303.

719 Wayment-Steele HK, Ojoawo A, Otten R, Apitz JM, Pitsawong W, Hömberger M,  
720 Ovchinnikov S, Colwell L, Kern D. 2023. Predicting multiple conformations via  
721 sequence clustering and AlphaFold2. *Nature*:1–3.

722 Whelan S, Liò P, Goldman N. 2001. Molecular phylogenetics: state-of-the-art methods  
723 for looking into the past. *Trends Genet.* 17:262–272.

724 Zhang N, Guan W, Cui S, Ai N. 2023. Crowded environments tune the fold-switching in  
725 metamorphic proteins. *Commun. Chem.* 6:117.

726

727

728

729

730

731

732